Dynamic Characteristic Analysis and LMI-based H_∞ Controller Design for a Line of Sight Stabilization System

Won Gu Lee
Research Institute of Mechanical Technology, Pusan National University, Pusan 609-735, Korea
In Soo Kim
Graduate School of Mechanical and Intelligent Systems Engineering, Pusan National University, Pusan 609-735, Korea
Joong Eup Keh
Defense Quality Assurance Agency, Pusan, Korea
Man Hyung Lee*
School of Mechanical Engineering and ERC/Net Shape & Die Manufacturing, Pusan National University, Pusan 609-735, Korea

This paper is concerned with the design of an LMI(Linear Matrix Inequality)-based H_∞ controller for a line of sight(LOS) stabilization system and with its robustness performance. The linearization of the system is necessary to analyze various nonlinear characteristics, but the linearization entails modeling uncertainties which reduce its performance. In addition, the stability of the LOS can be adversely affected by angular velocity disturbances while the vehicle is moving. As the vehicle accelerates, all the factors that are ignored and simplified for the linearization tend to inhibit the performance of the system. The robustness in the face of these uncertainties needs to be assured. This paper employs H_∞ control theory to address these problems and the LMI method to provide a suitable controller with minimal constraints for the system. Even though the system matrix does not have a full rank, the proposed method makes it possible to design a H_∞ controller and to deal with R and S matrices for reducing the system order. It can be also shown that the proposed robust controller has a better disturbance attenuation and tracking performance. The LMI method is also used to enhance the applicability of the proposed reduced-order H_∞ controller for the system given. The LMI-based H_∞ controller has superior disturbance attenuation and reference input tracking performance, compared with that of the conventional controller under real disturbances.

Key Words: Line of Sight(LOS), Gimbal, Linear Matrix Inequality(LMI), H_∞ Control

1. Introduction

Modern military vehicles are have becoming ever more sophisticated and automated through scientific and technical advancements. The line of sight(hereafter we call it a LOS) stabilization system mounted on ground vehicles is operated as both a synthetic sensor package and mechanical stabilization system. Though a vehicle may move in a certain direction, its LOS stabilization system enables the operator to fire at a target with accurate recognition and tracking. The LOS stabilization system plays an important role in tracking the target and following the operator's handle command in a stable manner. Thus, it is also important to ensure the stability of the LOS for the operator and to send the tar-

* Corresponding Author,
E-mail : mahlee@hyowon.ac.kr
TEL : +82-51-510-2331; **FAX** : +82-51-512-9835
School of Mechanical Engineering and ERC/Net Shape & Die Manufacturing, Pusan National University, Pusan 609-735, Korea. (Manuscript **Received** October 16, 2000; **Revised** June 26, 2002)

get's position into fire-control system(Iecovich, 1990). In the guidance system, the LOS stabilization system enables the operator to control the gun and turret by accurately tracking the target (Iecovich, 1990 ; Lee, 1990). The system tasks are achieved through an angular velocity control loop that uses the gyro which acts as an inertial sensor. Moreover, these servo and stabilization functions of the system are closely related to the magnitude of the disturbance and controller. Most stabilization errors of the system usually lie between 0.25 mil and 0.05 mil. There are numerous disturbances such as bearing friction, mass unbalance, spring force(by sensor and actuator) and othey forces(by the moment of inertia and geometry). The loearing friction deteriorates the tracking performance at low speed and adversely affects the stability(Li, et al., 1994). Techniques for nonlinear control have been studied in the LOS stabilization system(Keh, et al., 1999 ; Lee, et al., 1999). Most nonlinear controllers have some advantages in that they demand no linear model and have quick response, but they have inadequate robustness against severely varying disturbances and modeling uncertainties. Adequate robustness is needed to guarantee that an operator could aim at a target and fire it accurately under real disturbances in the field. The recent study has focused on attenuating real disturbances, improving the tracking performances and reducing the necessity for trouble shooting in the velocity control system(Iecovich, 1990 ; Lee, 1990 ; Li, et al., 1994 ; Jeon, 1997).

2. LOS Stabilization System

The LOS stabilization system is used as an electro-optical device mounted on the turret not only for tracking a moving target, but for keeping the LOS in a stable position. The LOS should have sufficient stability to satisfy the robustness of the system. The LOS stabilization system has two functions : One is a servo function to track the target in a stable manner while in motion. The other is a stabilization function to stabilize the LOS in order to accomodate the torque input provided by the operator.

2.1 Structure of the LOS stabilization system

2.1.1 LOS stabilization system

The main system is shown in Fig. 1 and consists of a gimbal housing, a platform, a mirror, and an inertial balancer. The gimbal is a belt-driven system with simple mechanism, and the inertial balancer is used to enhance the stability of the LOS inside.

The following assumptions are made :

(1) The rotational friction could be ignored at each rotation axis,

(2) The stiffness of wire band has an infinite value and has no slip,

(3) The motion of base structure could be measured,

(4) Only the elevation motion exists.

Based on the alove assumptions, the following relations can be established

$$\gamma_b\omega_{b/t} = -\gamma_m\omega_{m/t},\ \gamma_m\omega_{m/t} = -\gamma_p\omega_{p/t} \qquad (1)$$

where the subscripts b, m and p stands for the band, the mirror and the platform, respectively. The relative angular velocity is defined as follows

$$\begin{aligned} \omega_{m/t} &= \omega_m - \omega_t \\ \omega_{p/t} &= \omega_p - \omega_t \\ \omega_{b/t} &= \omega_b - \omega_t \end{aligned} \qquad (2)$$

When a kinetic energy of the system can be obtained by the given geometric relations, the equation of motion is expressed by applying the Lagrange's method(Kim, et al., 1990) as follows

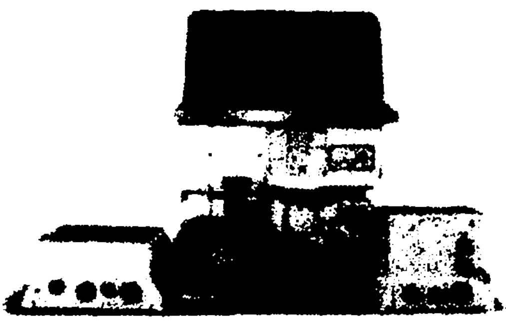

Fig. 1 A line of sight stabilization system

$$J_m\dot{\omega}_m+\frac{J_p r_m-(r_m\dot{\omega}_m-(r_m-r_p)\dot{\omega}_t)}{r_p^2}+\frac{J_b r_m-(r_m\dot{\omega}_m-(r_b-r_m)\dot{\omega}_t)}{r_b^2}=0 \quad (3)$$

Eg. (3) is rearranged into the following equation of the angular velocity of the mirror

$$\dot{\omega}_m=\dot{\omega}_t\frac{\left\{\frac{r_m}{r_p}\left(\frac{r_m}{r_p}-1\right)J_p+\frac{r_m}{r_b}\left(\frac{r_m}{r_b}-1\right)J_b\right\}}{J_m+J_p\left(\frac{r_m}{r_p}\right)^2+J_b\left(\frac{r_m}{r_b}\right)^2} \quad (4)$$

The angular acceleration in (4) should have a value that is one-half of that of base structure in order to stabilize the LOS.

$$\dot{\omega}_m=\frac{1}{2}\dot{\omega}_t \quad (5)$$

where the ratio of the radius of the drive shaft of the mirror to that of the platform can be determined as follows

$$\frac{r_m}{r_p}=2 \quad (6)$$

Therefore, J_b, the moment of the inertia of inertial balancer by applying Egs. (4), (5), and (6) can be represented as follows

$$J_b=\frac{J_m}{\frac{r_m}{r_b}\left(\frac{r_m}{r_b}+2\right)} \quad (7)$$

where the radius of the drive shaft of the inertial balancer would be predetermined by geometric relations, and the variables of the mirror can be also determined. Hence, the moment of inertia in the inertial balancer would be obtained by (7).

2.1.2 Stabilization mode

The operation mode can be divided into three modes; stabilization, tracking and auto-drift compensating mode. But, here only the stabilization mode will be introduced for the experiments. The stabilization mode includes an angular velocity control loop as well as an important operation mode related with the motion of the vehicle.

The specifications of the design are shown in Table 1. The proposed controller can be designed when all components of the stabilization system are designed and tested.

2.2 Mathematical modeling

With the kinetic energy of the rigid body and the elastic energy of wire band included in deriving the equation of motion, the following equation can be obtained by applying the Lagrange's method (Lee, et al., 1999).

$$\frac{d}{dt}\left(\frac{\partial(T-V)}{\partial\dot{q}_i}\right)-\frac{\partial(T-V)}{\partial q_i}=Q_i \quad (8)$$

Before deriving the equation of motion, the following assumptions should be taken. First, the center of gravity of the gimbal housing, platform, mirror and inertial balancer lie on the same plane. Second, the center of gravity should coincide with the center of rotation. Finally, the angular velocity can be measured.

2.3 Nonlinear equation of motion

The rectangular coordinates attached to each rigid body are used for deriving simple equations

Table 1 Design performance of stabilization mode

Contents	Objectives	Remarks
Bandwidth	Over 30Hz	
Velocity of motion at elevation	Max. over 10°/sec Min. below 0.25 mil/sec	
Velocity of motion at azimuth	Max. over 40°/sec Min. below 0.25 mil/sec	
Stabilization accuracy	Below 0.1 mil RMS	
Tracking accuracy	Below ±1.5% or ±0.3 mil	
Drift	Below 0.2 mil/sec	
Acceleration capability	Over 3 rad/sec²	

2.3.1 Dynamic equations

A. Kinetic energy

The overall kinetic energy of the system can be represented as (9) by adding up the kinetic energies of each rigid body (Li, et al., 1994).

$$
\begin{aligned}
T &= T_G + T_P + T_M + T_B \\
&= \frac{1}{2} m_G \sum_{i=1}^{3} V_i^{G*} V_i^{G*} + \frac{1}{2} \sum_{i=1}^{3} G_i \omega_i^G \omega_i^G \\
&\quad + \frac{1}{2} m_P \sum_{i=1}^{3} V_i^{P*} V_i^{P*} + \frac{1}{2} \sum_{i=1}^{3} P_i \omega_i^P \omega_i^P \\
&\quad + \frac{1}{2} m_M \sum_{i=1}^{3} V_i^{M*} V_i^{M*} + \frac{1}{2} \sum_{i=1}^{3} M_i \omega_i^M \omega_i^M \\
&\quad + \frac{1}{2} m_B \sum_{i=1}^{3} V_i^{B*} V_i^{B*} + \frac{1}{2} \sum_{i=1}^{3} B_i \omega_i^B \omega_i^B
\end{aligned} \tag{9}
$$

B. Potential energy

The potential energy of the system is divided into two parts : One is an elastic energy V_k due to the wire band and the other is a potential energy V_g due to the gravity. The elastic energy (Li, et al., 1994) due to the wire band with its stiffness can be represented as follows

$$
\begin{aligned}
V_k &= \frac{1}{2} K_1 (r_P \theta_P - r_M \theta_M)^2 + \frac{1}{2} K_2 (r_B \theta_B - r_P \theta_P)^2 \\
&\quad + \frac{1}{2} K_3 (r_M \theta_M - r_B \theta_B)^2
\end{aligned} \tag{10}
$$

$$
K_1 = \frac{EA}{L_1}, \quad K_2 = \frac{EA}{L_2}, \quad K_3 = \frac{EA}{L_3}
$$

where E and A are the coefficients of the wire band and the area, and L_1, L_2 and L_3 are the lengths of the band between the platform and the mirror, between the platform and the inertial balancer, and between the inertial balancer and the mirror, respectively. In addition, the potential energy due to the gravity (Li, et al., 1994) can be given by

$$
\begin{aligned}
V_{gM} &= -(\underline{m_0} + \underline{m}) \cdot m_M g (-\underline{k}) \\
V_{gG} &= -\underline{g_O} \cdot m_G g (-\underline{k}) \\
V_{gB} &= -\underline{b_O} \cdot m_B g (-\underline{k}) \\
V_{gP} &= -(\underline{P_O} + \underline{P}) \cdot m_P g (-\underline{k})
\end{aligned} \tag{11}
$$

Thus, the to tal potential energy V of the system is equal to the sum of (10) and (11).

$$
V = V_k + V_{gM} + V_{gG} + V_{gB} + V_{gP} \tag{12}
$$

C. Generalized forces

The generalized coordinates q_i are the rotation angles θ_G, θ_P and θ_B, and the generalized forces with regard to the generalized coordinates can be represented as follows

$$
\begin{aligned}
G_{\theta_G} &= T_{mG} - \tau_{fG} \\
Q_{\theta_P} &= T_{mP} - \tau_{fP} \\
Q_{\theta_B} &= -\tau_{fB} \\
Q_{\theta_M} &= -\tau_{fM}
\end{aligned} \tag{13}
$$

where T_{mG} and T_{mP} denote the external torques needed for rotating the gimbal housing in the azimuth and the platform in the elevation direction, resgectively.

2.3.2 Linearization and simplification

The equation of motion can be solved by using the Lagrange Eq. (8) and the nonlinear equation of motion for the generalized coordinates θ_M, θ_P, θ_B and θ_G is given in (Li, et al., 1994). The given nonlinear equation can be simplified and linearized by the following assumptions.

First, there is no motion of a base structure, that is,

$$
V^s = \omega^s = 0 \tag{14}
$$

Second, the wire band's stiffness is infinite, for the friction can be identified at low frequency range,

$$
r_B \theta_B = r_M \theta_M = r_P \theta_P \tag{15}
$$

Also, the gimbal can be decoupled in each direction ; i.e., it can be driven independently. Therefore, the equation of motion can be simplified as follows

$$
J_A \ddot{\theta}_G + \tau_{fG} = T_{mG} \tag{16}
$$

$$
J_E \ddot{\theta}_P + \tau_{fE} = T_{mP} \tag{17}
$$

where J_A and J_E are the moments of inertia, and τ_{fG} and τ_{fE} are the frictions in each direction. The moment of inertia for azimuth and elevation can be represented as follows

$$
\begin{aligned}
J_A &= G_3 + B_3 + P_3 + M_3/2 + M_2/2 + m_B b_2^2 \\
&\quad + m_G g_2^2 + m_M m_2 (m_2 + m/\sqrt{2}) \\
&\quad + m_P p_2 (p_2 - p)
\end{aligned} \tag{18}
$$

$$
\begin{aligned}
J_E &= P_1 + m_P p^2 + (M_1 + m_M m^2) \left(\frac{r_M}{r_P} \right)^2 \\
&\quad + B_1 \left(\frac{r_B}{r_P} \right)^2
\end{aligned} \tag{19}
$$

Only the Coulomb friction f_c is considered and

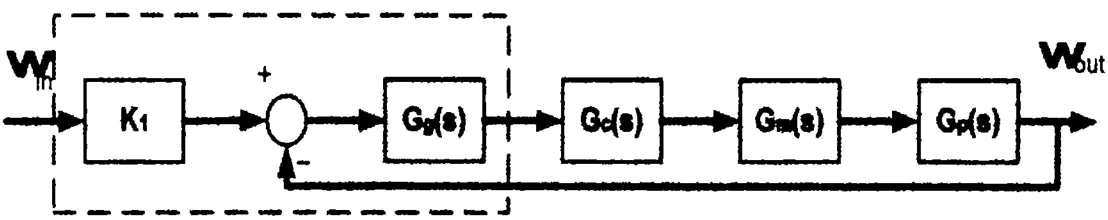

Fig. 2 Velocity control loop in a LOS stabilization system

its magnitude is proportion al to the moment of inertia.

The angular velocity control loop can be shown in Fig. 2.

A. Gyro

The gyro is one of two-axes DTGs(dynamically tuned gyro) and is represented with a dotted line in Fig. 2. The reference mode with a large bandwidth is used in this system. Its precession scale factor K_1 converts 10 V into 40°/sec and 10 V into 10°/sec respectively. Its dynamics and integrators are also shown in Fig. 2 and its transfer function is obtained from the magnitude and the phase information for given frequency range by curve-fitting each transfer function. Moreover, the output of the integrator has an anguler scale of 30 V_{dc}/deg as

$$G_g(s) = \frac{4901463072.8}{s^3+2419.3s^2+4544462.8s+49167562.8} \cdot \frac{1718.8}{s} \tag{20}$$

B. Motor

The motor is one of the actuators which drive the plant by the control output with the high bandwidth, the small ripple, the linear gain characteristics and the sufficient torque. The bandwidth and its gain can be obtained by designing a power amplifier. However, its dynamics may be ignored, for its bandwidth is set up 10 times as that of the system. In other words, it can be considered as a constant gain in Fig. 2.

$$G_m(s) = 17$$

C. Plant

As previously mentioned, the plant of the system is a gimbal, which has large stiffness and low ratio of the friction to the moment of inertia. In particular, the friction can be regarded as a torque disturbance. The characteristics of the friction is time-variant and the moment of inertia may be just considered with the controller design.

$$G_P(s) = \frac{1}{4.82s+2.4} \tag{21}$$

D. Controller

The controller in the stabilization mode is designed by considering the bandwidth and the relative stability of the system, where the bandwidth is 30 Hz and the values for the relative stability are 3.3 dB and 25.5° for the gain and phase margin, respectively. The structure, in general, can be represented as a PI-Lead controller and the output of the integrator should be constrained at 2 V of the controller to prevent the windup.

$$G_C(s) = \frac{127.9(s+0.63)(s+8.2)}{s(s+4317.3)} \tag{22}$$

3. Analyses and Experiments on Stabilization Performance

Figure 3 shows the experimental device setup for obtaining step responses of the stabilization and the tracking modes and the experimental data can be shown on the oscilloscope and the plotter. The following step response with amplitude 1 V and duty cycle 50% illustrates each step response in the stabilization and the tracking mode. The settling time in the stabilization mode is smaller than that of the follow mode as seen in Fig. 4 and Fig. 5, and also the stabilization mode has a better performance at low frequency range.

Fig. 3 Equipment setup for acquiring the experimental data

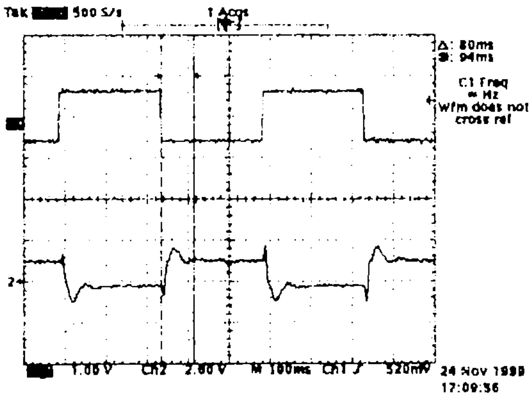

Fig. 4 Step response at an azimuth in the tracking mode

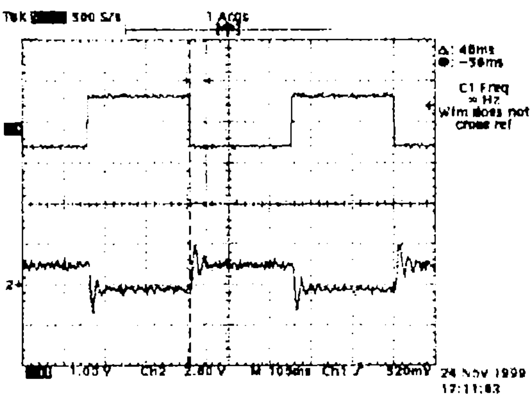

Fig. 5 Step response at an azimuth in the stabilization mode

3.1 Experimental device setup

The experiment is supposed to be conducted on

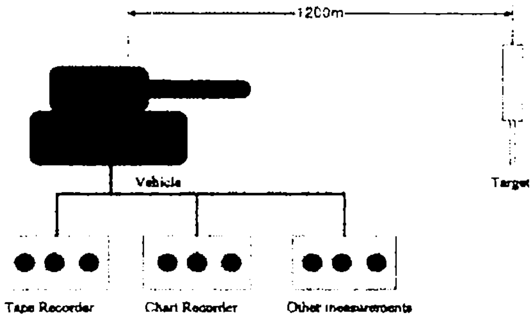

Fig. 6 Configuration for the experiments attached to the vehicle

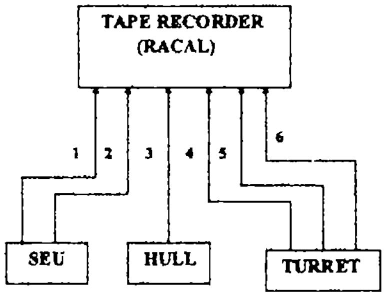

1 : Gyro signal at an azimuth
2 : Gyro signal at an elevation
3 : Vehicle Gyro signal at an azimuth
4 : Turret Gyro signal at an elevation
5 : DCT signal at an azimuth
6 : DCT signal at an elevation

Fig. 7 Signal flow for signal acquisitions

two standard driving courses ; i.e., it would be conducted on paved and bumpy courses. The vehicle used is one of the prototypes of military Korean tank and the target is a square mark with the length of 2.3 m and is far away the forward distance of 1200 m. The measuring devices are used with the vehicle's battery as a power supply and are linked with recorder and other measurement devius. The experimental setup is illustrated in Fig. 6.

The tests of the stabilization performance while moving are conducted for both the paved and bumpy courses, and are also measured for the output of the gyro in the reference mode and for the input of the angular velocity disturbance. A tape recorder is used to obtain the experimental data, and the experiments are performed at 20 KPH and 40 KPH in the paved course and

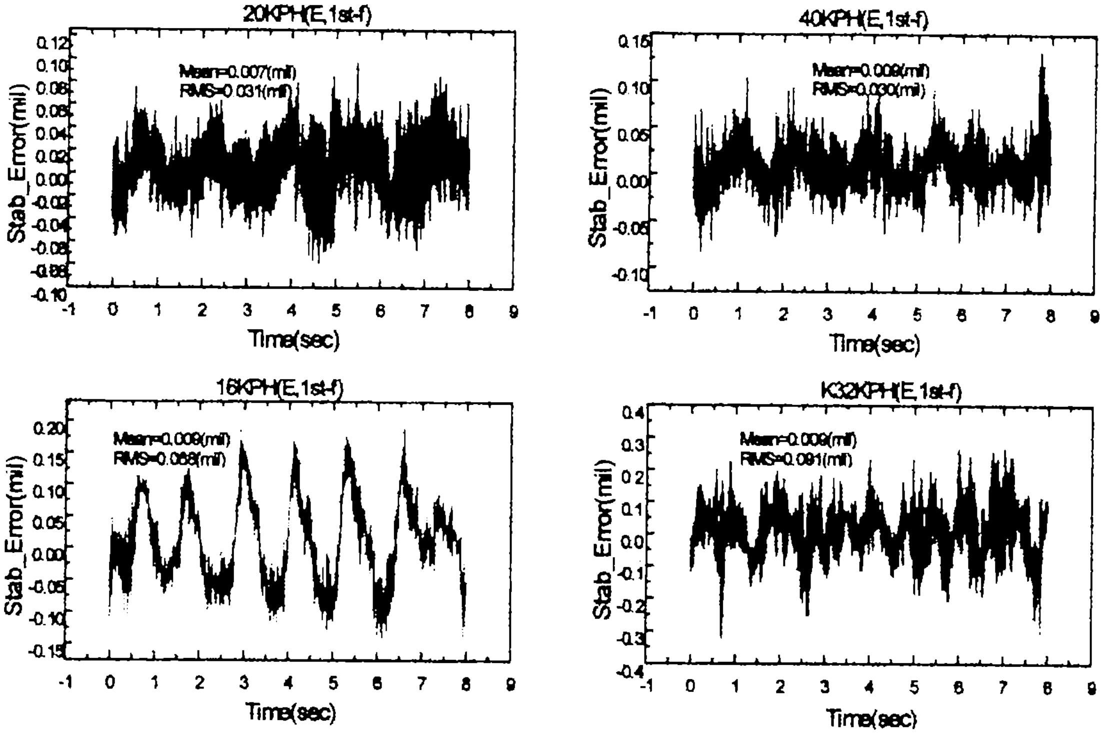

Fig. 8 Stabilization errors at each velocity in the elevation direction

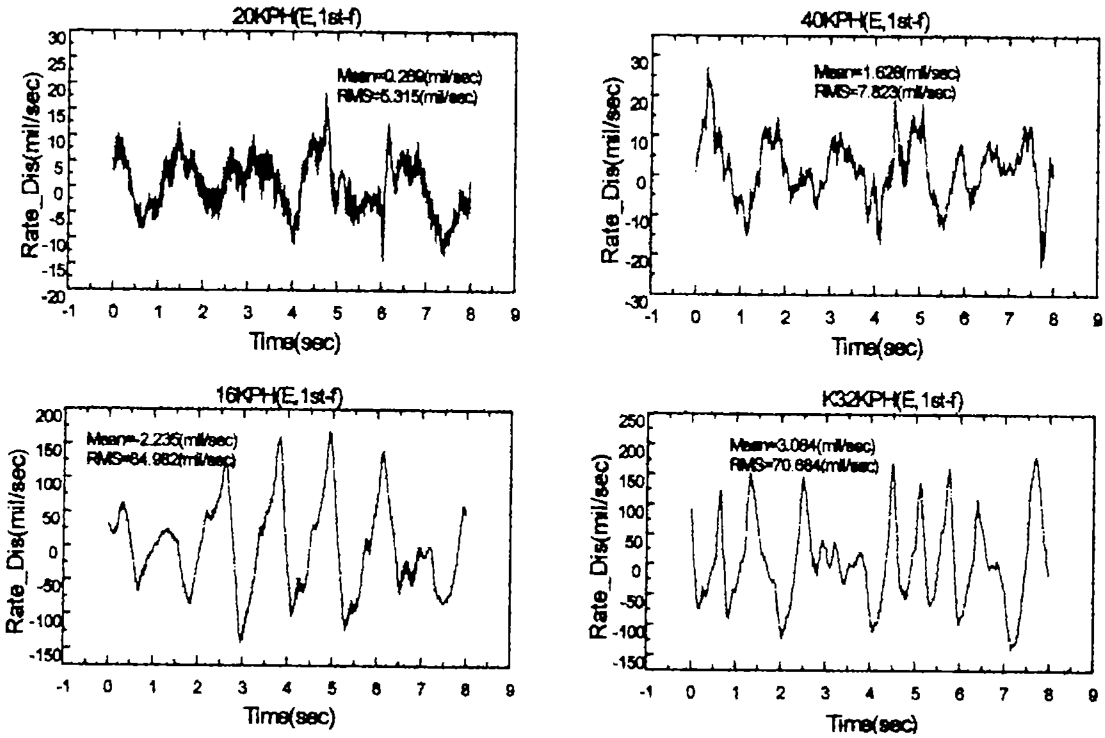

Fig. 9 Disturbances at each velocity in the elevation direction

16 KPH and 32 KPH in the bumpy course. Each signal is acquired as in Fig. 7.

3.2 Time signal analysis

This section provides the magnitude of real disturbances and the characteristics of stabilization performances for time signal analysis, and the experimental data are shown in Fig. 8 and Fig. 9. The errors and the disturbances in the stabilization are shown in Table 2.

Heve, P-P means the difference between the maximum and the minimum value, and RMS stands for the root mean square.

3.3 Frequency signal analysis

The acquired data are analyzed to determine the stabilization performance and the angular velocity disturbance in Table 3 and Table 4, and the frequency responses in the elevation direction are shown in Fig. 10 and Fig. 11. It can be observed that electrical noises are pusent at 30 Hz and 60 Hz as seen in all figures.

Table 2 Angular velocity disturbances and stabilization error

Contents	No.	Paved Course		Bumpy Course	
		20 km/h	40 km/h	16 km/h	32 km/h
Stabilized Error at El. (mil)	Mean	0.007	0.009	0.009	0.009
	RMS	0.031	0.030	0.068	0.091
	P-P	0.176	0.192	0.330	0.547
Disturbance (mil/sec)	Mean	0.269	1.628	−2.235	3.084
	RMS	5.315	7.823	64.982	70.684
	P-P	29.329	43.417	301.702	321. 378

Table 3 Frequency signal analysis in the elevation direction the paved course

Contents	20 KPH	40 KPH
Stabilization (EL DTG)	- Dominant Peak : 30.3, 60, 89.5, 188, 304, 516, 960, 1280 Hz - High Power at 30∼60 Hz - High Power in low frequency	- Dominant Peak : 188, 252, 296, 516, 960, 1280 Hz - High Power at 62.3∼64.5 Hz and at 30∼60 Hz - High Power in low frequency
Angular velocity disturbance (TURRET F/F G.)	- Dominant Peak : 30, 60, 90, 400, 800 Hz : 800∼1000 Hz - Low Power in overall frequency - High Power below 60 Hz	- Dominant Peak : 256, 400, 628, 800 Hz :800∼1000 Hz : 62.5∼64.5 Hz - High Power below 60Hz

Table 4 Frequency signal analysis in the elevation on the bumpy course

Contents	16 KPH	32 KPH
Stabilization (EL DTG)	- Dominant Peak : 0.75, 192, 304, 336, 400, 516, 960, 1280 Hz : 24∼28 Hz - High Power at 25∼55 Hz	- Dominant Peak : 1, 108, 300, 400, 516, 596, 640, 680, 964, 1280 Hz - High Power at 37∼48 Hz - Some Power below 100 Hz
Angular velocity disturbance (TURRET F/F G.)	- Dominant Peak : 0.75, 252, 400, 800, 1280 Hz - High Power below 23∼28 Hz 60Hz	- Dominant Peak : 1, 400, 800, 1200, 1600 Hz - High Power below 100 Hz

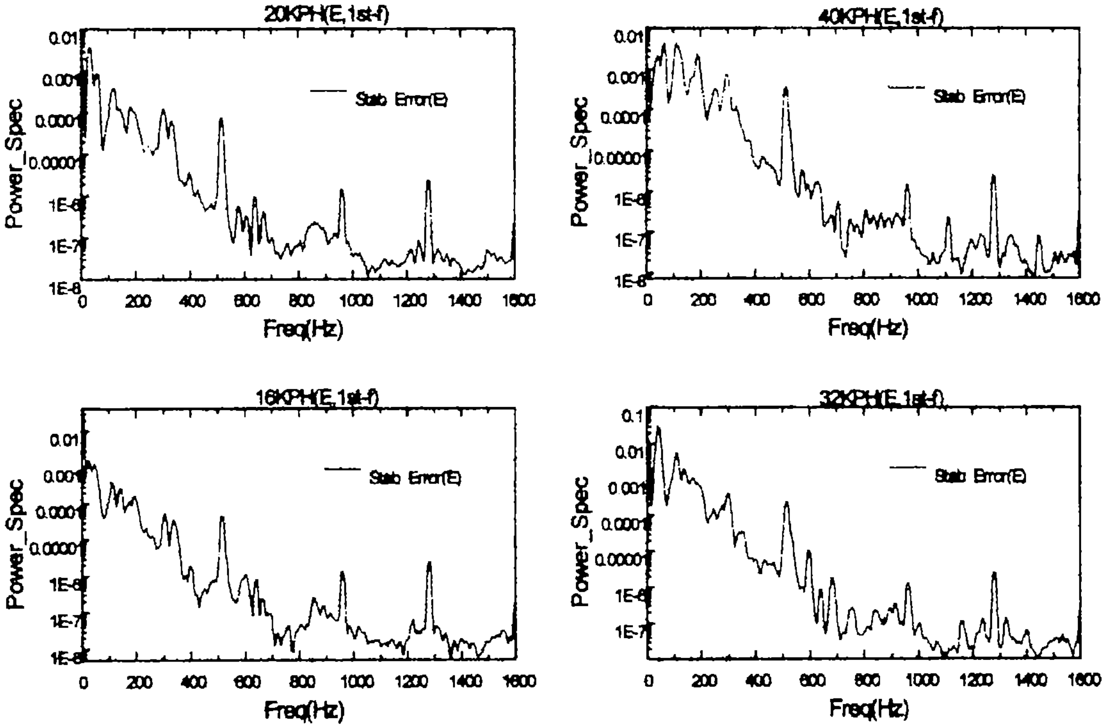

Fig. 10 Stabilization errors in the elevation direction.

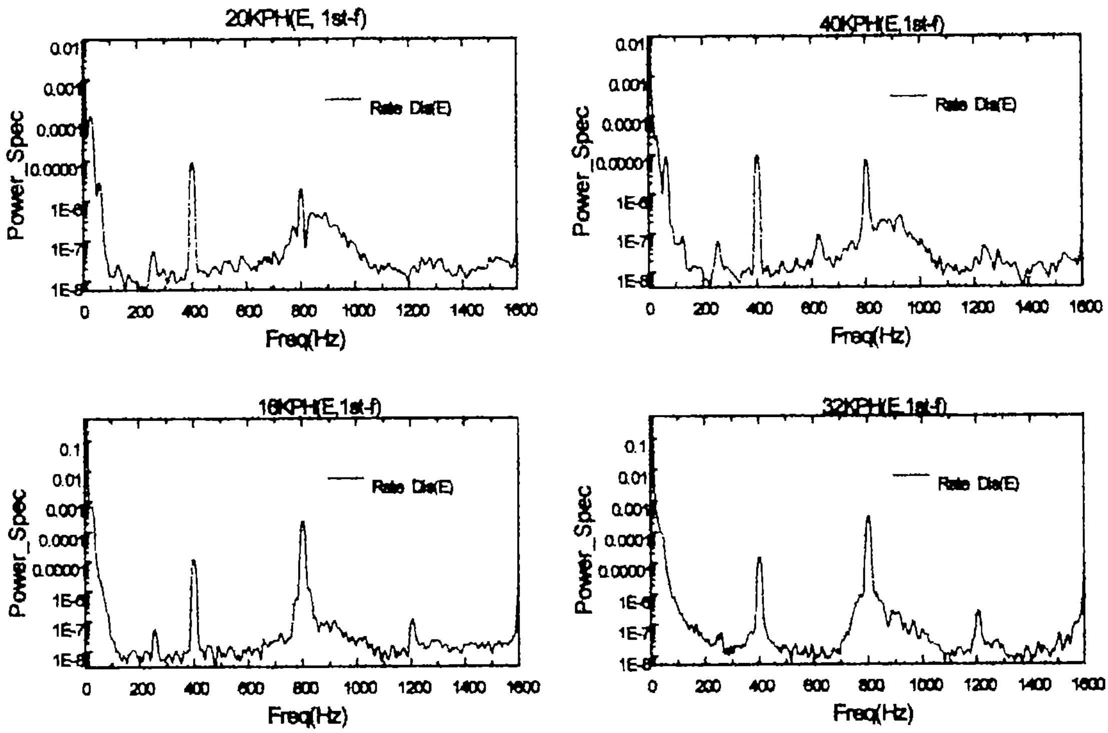

Fig. 11 Angular velocity disturbances in the elevation direction.

4. LMI-based H_∞ Controller Design

4.1 LMI-based H_∞ control

A set of H_∞ controllers with closed-loop performance γ can be implicitly parameterized by the solution (R, S) of a system of LMI (Gahinet, et al., 1994). The matrices R and S play a role analogous to that of the Riccati solutions and X_∞ and Y_∞ in classical Riccati-based H_∞ control (Doyle, et al., 1989). Useful applications include LMI-based H_∞ synthesis, mixed H_2/H_∞ design, and H_∞ design with a pole-placement constraint (Zhou, et al., 1994). This section is concerned with a reliable computation of H_∞ controllers given solution (R, S) of the characteristic system of LMIs.

Given a linear time-invariant plant $P(s)$ with state-space equations

$$\begin{aligned} \dot{x} &= Ax + B_1 w + B_2 u \\ z &= C_1 x + D_{11} w + D_{12} u \\ y &= C_2 x + D_{21} w \end{aligned} \tag{23}$$

consider a proper continuous-time plant $P(s)$ of order n and realization (23) and let N_{12} and N_{21} denote orthonormal bases of the null spaces of (B_2^T, D_{12}^T), (C_2, D_{21}) respectively. The sub-optimal H_∞ problem of performance γ is solvable if and only if there exist two symmetric matrices $R, S \in R^{n\times n}$ ying the following system of LMIs.

$$\begin{gathered} \left(\begin{array}{c|c} N_{12} & 0 \\ \hline 0 & I \end{array}\right)^T \left(\begin{array}{cc|c} AR+RA^T & RC_1^T & B_1 \\ C_1 R & -\gamma I & D_{11} \\ \hline B_1^T & D_{11}^T & -\gamma I \end{array}\right) \left(\begin{array}{c|c} N_{12} & 0 \\ \hline 0 & I \end{array}\right) < 0, \\ \left(\begin{array}{c|c} N_{21} & 0 \\ \hline 0 & I \end{array}\right)^T \left(\begin{array}{cc|c} A^T S+SA & SB_1 & C_1^T \\ B_1^T S & -\gamma I & D_{11}^T \\ \hline C_1 & D_{11} & -\gamma I \end{array}\right) \left(\begin{array}{c|c} N_{21} & 0 \\ \hline 0 & I \end{array}\right) < 0, \\ \begin{pmatrix} R & I \\ I & S \end{pmatrix} > 0 \end{gathered} \tag{24}$$

Considering the solutions (R, S) of the LMI system, (23)-(24) is a convex optimization problem. Efficient polynomial-time algorithms are now available to solve this LMI feasibility problem. Any feasible pair (R, S) determines a set of full-order γ-suboptimal controllers as follows. First compute via SVD two invertible matrices $M, N \in R^{n\times n}$ such that

$$MN^T = I - RS \tag{25}$$

The bounded real lemma matrix X_{cl} is then uniquely determined by the following equations.

$$X_{cl} =: \begin{pmatrix} S & N \\ N^T & * \end{pmatrix},\ X_{cl}^{-1} =: \begin{pmatrix} R & M \\ M^T & * \end{pmatrix}, \tag{26}$$
$$R, S, M, N \in R^{n\times n}$$

Specifically, X_{cl} is the unique solution of the linear equation

$$X_{cl} \begin{pmatrix} R & I \\ M^T & 0 \end{pmatrix} = \begin{pmatrix} I & S \\ 0 & N^T \end{pmatrix} \tag{27}$$

Note that (23) ensures that $X_{cl} > 0$. Once X_{cl} is determined, an adequate full-order controller is any solution of the controller LMI. In many linear control problems, the design constraints have a simple reformulation in terms of LMI, and especially Lyapunov techniques play a central role in the analysis and control of linear systems. The H_∞ control problem is a good illustration of this point. The H_∞ constraints can be expressed as a single matrix inequality via the bounded real lemma (BRL). The instrumental role of this lemma was first recognized in its inequality form. Even though the H_∞ control problem has an analytic solution in terms of Riccati equations, the LMI approach remains valuable for several reasons (Gahinet, et al., 1994; Iwasaki, et al., 1994, and the references therein).

First, it is applicable to all plants without restrictions on infinite or pure imaginary invariant zeros. Second, it offers a simple and insightful derivation of the Riccati-based solvability conditions. Third, it is practical thanks to the availability of efficient convex optimization algorithms. Finally, the LMI approach yields a e-dimensional parameterization of all H_∞ controllers with clear connections between all free parameters and the closed-loop Lyapunov function. Consequently, it offers numerically tractable means of exploiting the remaining degrees of freedom to reduce the controller order, to handle additional constraints on the closed-loop poles, and to design stable controllers, etc. Explicit formulas have been derived for LMI-based H_∞

controllers in continuous time contexts. These formulas are particularly suited for numerically stable implementation and bring insight into the controller structure (Zeren, et al., 1999). They have been successfully implemented in the LMI Control Toolbox in MATLAB (Gahinet, et al., 1995).

4.2 Requirements for controller design

The H_∞ controller for a given system is designed to satisfy the design specifications. In particular, the angular velocity should clesely follow the operator's command. In addition, the H_∞ controller is necessary to attenuate unexpected disturbances and parametric changes in the stabilization system.

A. Angle of gimbal's motion

The range of gimbal's motion should be between $-10°$ and $20°$ in the elevation direction on the side of the mirror, and should be between $-3°$ and $3°$ in the azimuth direction.

B. Static position accuracy of mirror in tracking mode

In the case that the mirror is attached to the turret, the accuracy of the static position from the electrical signal to the LOS should be constrained as follows.

Elevation : $-10° < \varepsilon < 20°$ error

$\triangle\varepsilon$: Max. 0.25 mil

Azimuth : $-3° < \eta 3°$ error

$\triangle\eta$: Max. 0.20 mil

C. Velocity of the LOS motion

The mirror should provide the minimum 10°/s in the elevation and the minimum 40°/s in the azimuth direction.

D. LOS tracking accuracy

In the range of gimbal's angles between $-10°$ and $20°$ in the elevation direction, and between $-3°$ and $3°$ in the azimuth direction, the error betweer the velocity input command and the actual LOS velocity should not exceed the maximum ; i.e., it should be smaller than 0.3 mil/s (or 1.5%).

E. Drift of the LOS

The drift in the gyro is adjusted on each axis within 5 minutes after the power is turned on and then the mean of drifts which are measured after the subseguent 5 minutes have elapsed should not exceed ± 0.025 mil/s. The range of the drift adjustment should not be smaller than ± 1 mil/s.

F. Bandwidth of stabilization mode loop

The bandwidth should not be smaller than 30 Hz or both axes.

G. Bandwidth of follow mode loop

The bandwidth should be at least 10 Hz in both axes.

4.3 Formulation of LMI-based H_∞ controller problem

As previously constructed the design specifications given for H_∞ controller, the generalized plant is shown in Fig. 12.

Where $G_o(s)$ is the nominal model with the motor and the gimbal as the control plant, $W_1(s)$ and $W_2(s)$ are the weighting functions for the input and output of $G_o(s)$ respectively, and $K(s)$ is a designed H_∞ controller. Also, let r be the reference input and w_1 and w_2 be the plant input disturbances serving as the external input, and z_1 and z_2 be the control objectives serving as the error between the outputs and the control inputs u. In addition, let $G_{zw}(s)$ be a closed-loop transfer function from w_1, w_2 and u to z_1, z_2 and y.

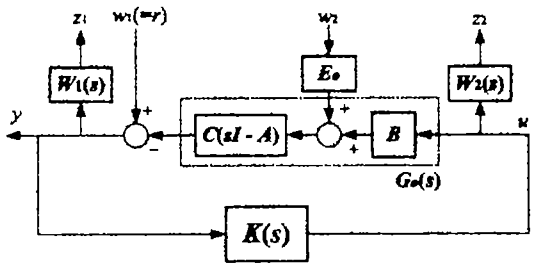

Fig. 12 The generalized plant for H_∞ controller design

$$\begin{bmatrix} z_1 \\ z_2 \\ y \end{bmatrix} \begin{bmatrix} W_1(s) & W_1(s)E(s) & W_1(s)G(s) \\ 0 & 0 & W_2(s) \\ I & E(s) & G(s) \end{bmatrix} \begin{bmatrix} w_1 \\ w_2 \\ u \end{bmatrix} \quad (28)$$

where $E(s)$ is the transfer function from the disturbance w_2 to the plant output. By realizing the state variables for $G_o(s)$, $E(s)$, $W_1(s)$ and $W_2(s)$ into (24), the given generalized plant can be represented as the following state space model.

$$G_o(s) = \left[\begin{array}{c|c} A_o & B_o \\ \hline C_o & D_o \end{array}\right], \; E(s) = \left[\begin{array}{c|c} A_o & B_o \\ \hline C_o & E_o \end{array}\right]$$
$$W_1(s) = \left[\begin{array}{c|c} A_{w1} & B_{w1} \\ \hline C_{w1} & D_{w1} \end{array}\right], \; W_2(s) = \left[\begin{array}{c|c} A_{w2} & B_{w2} \\ \hline C_{w2} & D_{w2} \end{array}\right] \quad (29)$$

$$\dot{x} = \begin{bmatrix} A_{w1} & 0 & -B_{w1}C_o \\ 0 & A_{w2} & 0 \\ 0 & 0 & A_o \end{bmatrix} x + \begin{bmatrix} B_{w1} & 0 \\ 0 & B_{w2} \\ 0 & E_o \end{bmatrix} w + \begin{bmatrix} 0 \\ 0 \\ B_o \end{bmatrix} u \quad (30)$$

$$z = \begin{bmatrix} C_{w1} & 0 & -D_{w1}C_o \\ 0 & C_{w2} & 0 \end{bmatrix} x + \begin{bmatrix} D_{w1} & 0 \\ 0 & 0 \end{bmatrix} w + \begin{bmatrix} 0 \\ D_{w2} \end{bmatrix} u \quad (31)$$

$$y = [0 \;\; 0 \;\; -C_o] x + [I \;\; 0] w \quad (32)$$

4.4 Simulation results and remarks

The simulations are conducted as follows : Let w_1 be the angular velocity as a reference input triggered by an operator's handle input in Fig. 12, and w_2 be the step disturbance in Fig. 14. Also, actuel angular velocity disturbances measured from both the paved and bumpy courses are used in all simulations. To compare the performance of the proposed controller with that of the conventional controller, two cases could be considered in the elevation direction : One is the case with real disturbances and the other is with no disturbance. Figure 13 shows the step response of the proposed H_∞ controller, compared with that of the conventional PI-Lead controller with no disturbance. The maximum overshoot of H_∞ controller is 38% and the settling time is 0.09 second, while the maximum overshoot of PI-Lead controller is 60% and the settling time is 0.3 second. Thus, it can be known that the proposed H_∞ controller has better step response performance with no disturbance. The step response is also considered with some disturbances. Figure 14 presents step responses of PI-Lead controller and H_∞ controller when the angular velocity step disturbance of 0.5 mil/s is triggered at 1 second. For both controllers, the magnitudes the step response are decreased by 0.5 mil/s at that time. However, the H_∞ controller case shows almost error after 0.06 seconds, while PI-Lead controller cese still has a steady state error after 0.21 seconds. Therefore, it can be seen that the proposed H_∞ controller has superior disturbance attenuation performance.

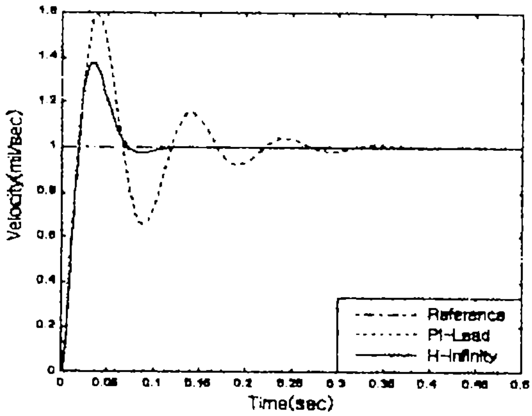

Fig. 13 Step response with no disturbance

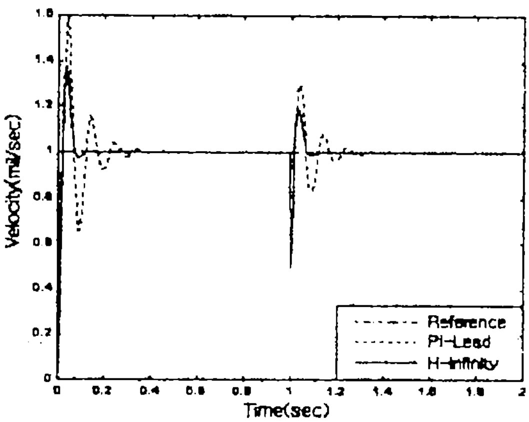

Fig. 14 Step response with a step-type output disturbance

The stabilization performance of the proposed LMI-based H_∞ controller and the conventional PI-Lead controller is verified with actual disturbances. The simulations to determine robust performances such as disturbance attenuation and reference input tracking can be conducted for the elevation direction. Figure 15(a) shows that the maximum overshoot of the proposed controller is smaller than that of PI-Lead controller, but they

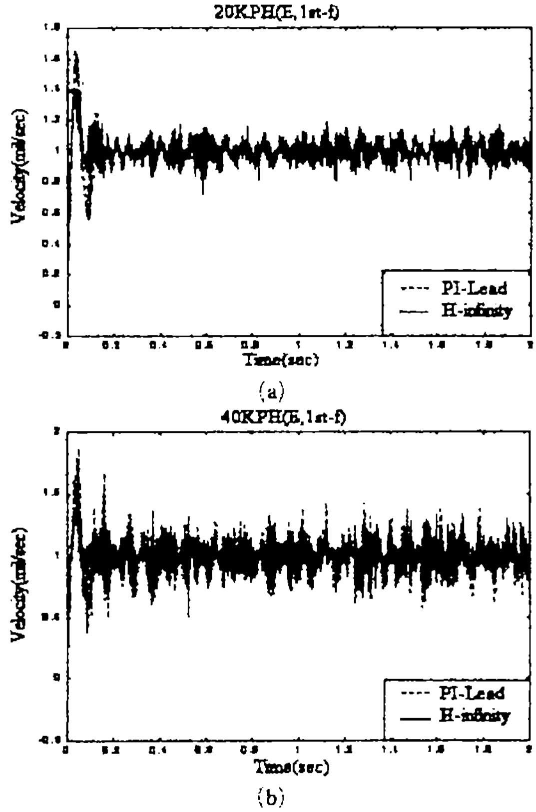

Fig. 15 Angular velocity response with the paved course disturbance ((a) 20 KPH (b) 40 KPH)

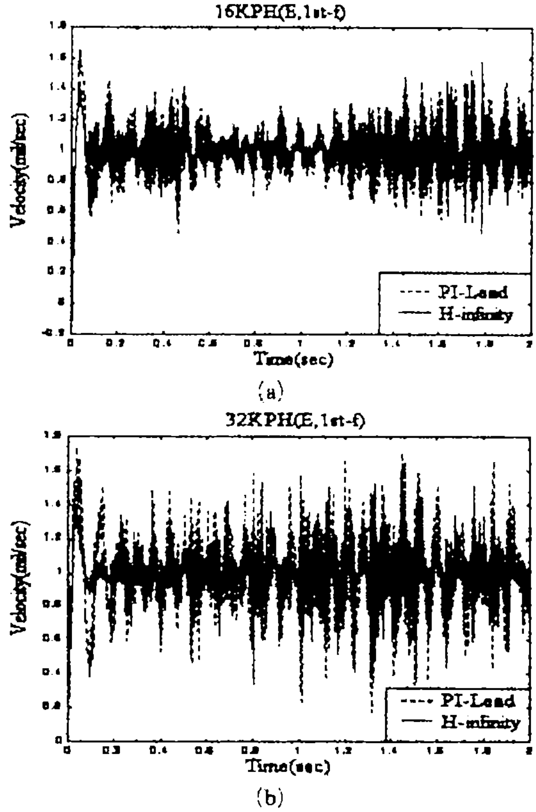

Fig. 16 Angular velocity response with the bumpy course disturbance ((a) 16 KPH (b) 32 KPH)

both have an overall response at 20 KPH on the paved course.

However, the faster the velocity of the vehicle, the worse is the response of PI-Lead controller. Moreover, Fig. 15(b) shows that the response of H_∞ controller is guite satisfactory, the responses of both controllers in Fig. 16 tend to deteriorate for faster motion and on ill-shaped courses, because the nonlinear effects of the system become more pronounced for faster motion. In addition, Since the ill-shaped courses have worse effects on the motion of vehicle, the controller can not have a good stabilization performance. Compared with the PILead controller, the proposed H_∞ controller has better robust ness performance under disturbances and nonlinear uncertainties.

Consequently, the results indicate that the proposed H_∞ controller has a better tracking performance for the reference input than that of the conventional PI-Lead controller.

5. Conclusions

It is necessary to design the robust controller to overcome disturbances and modeling errors of the system, so that the LOS stabilization system can achieve both a servo function and stabilization function independently. In this paper, nonlinear characteristics of the system are investigated through measured response characteristics such as the bandwidth, transient response and mirror chattering. The effects of the angular velocity disturbance are analyzed in both the time and frequency domains. In a controller design, the dynamics of the system needed to be accuratdy determimd in order to maintain a better LOS under a variety of disturbances, and the proposed control algorithm is reritied by numerous simulations with actual disturbances. In addition, the LMI-based H_∞ controller is designed to improve the robust ness performance against parametric changes, modeling errors and various disturbances. Also, the simulations have been conducted with actual disturbances. The following results have been obtained from the proposed robust control algorithm.

First, it can be confirmed that the proposed controller has better robust ness performance against nonlinear parametric changes and modeling errors. Second, the bandwidth in the azimuth direction is larger than that of the elevation direction and has a somewhat smaller relative stability, while it has a good tracking and mirror chattering performance for the step input transient response. Third, the stabilization performance has numerous effects on the target-hitting rate while in motion. It has a stable tracking performance for an input command of the ballistic trajectory calculator for both the angular velocity control in the stabilization mode and the angle control in the tracking mode, and has superior stabilization performance in the azimuth direction with disturbances. Fourth, excellent stabilization performance in the time and frequency domains can be obtained from the experiments for both the paved and bumpy courses. Finally, the proposed LMI-based H_∞ controller shows a good disturbance attenuation and reference input tracking performance, compared with that of the conventional controller under disturbances.

References

Doyle, J. C. Glover, K., Khargonekar, P. P. and Francis, B. A., 1989, "State-Space Solutions to Standard H_2 and H_∞ Control Problems," *IEEE Transactions on Automatic Control*, Vol. 34, No. 8, pp. 831~847.

Gahinet, P. and Apkarian, P., 1994, "A Linear Matrix Inequality Approach to H_∞ Control," *International Journal of Robust Nonlinear Control*, Vol. 4, pp. 421~448.

Gahinet, P., Nemirovski, A., Laub, A. J. and Chilali, M., 1995, LMI Control Toolbox, Math Works.

Iecovich, M., 1990, "Line of Sight Stabilization Requirements for Target Tracking Systems," *Proceedings of SPIE Acquisition, Tracking, and Pointing IV*, Vol. 1304, pp. 100~111.

Iwasaki, T. and Skelton, R. E., 1994, "All Controllers for the General H_∞ Control Problem : LMI Existence Conditions and State Space Formulas," *Automatica*, Vol. 30, No. 8, pp. 1307~1317.

Jeon, K. J., 1997, Design of Neural Network Control Next Generation Sight System, Samsung Electronics Co. Ltd.

Keh, J. E., Lee, W. G. and Lee, M. H., 1999, "Sliding Mode Control of the Gunner's Primary Stabilized Head Mirror," *Journal of the Korean Society of Precision Engineering*, Vol. 10, pp. 109~117. (in Korean)

Kim, C. H., Kim, S. S. and Shin Y. J., 1990, "A New Solution For Mechanisms Including Coulomb Friction," *KSME International Journal*, Vol. 4, No. 2, pp. 136~140.

Lee, M. H., 1990, The Study on Stabilization Characteristics and Control of Stabilized Head Mirror, Final Report to Agency for Defense Development.

Lee, W. G. and Lee, M. H., 1999, "Nonlinear Adaptive Control of a Line-of-Sight Stabilization System," *Proceedings of International Conference on Mechatronic Technology*, pp. 566~571.

Li, B., Hullender, D. and Direnzo, M., 1994, "Active Compensation for Gimbal Bearing Friction in Vibration Isolation and Inertial Stabilization Problems," *ASME Active Control of Vibration and Noise*, DE-Vol. 75, pp. 471~476.

Zeren, M. and Ozbay, H., 1999, "On the Synthesis of Stable H_∞ Controller," *IEEE Transactions on Automatic Control*, Vol. 44, No. 2, pp. 431~435.

Zhou, K., Glover, K., Bodenheimer, B. and Doyle, J., 1994, "Mixed H_2 and H_∞ Performance Objectives I : Robust Performance Analysis," *IEEE Transactions on Automatic Control*, Vol. 39, No. 8, pp. 1564~1574.